A Micromachined Wide-Bandwidth Magnetic Field Sensor Based on All-PMMA Electron Tunneling Transducer

Jing Wang, Wei Xue, Naidu V. Seetala, Xueyuan Nie, Efstathios I. Meletis, and Tianhong Cui

***Abstract*—All-PMMA-based tunneling magnetic sensors were fabricated by hot embossing replication with silicon templates. The silicon templates had smooth surfaces, positive profiles, and pyramid-like pits with a high aspect ratio. With this fast (20 min), simple (one-step), and repeatable method, the all-PMMA tunneling sensor platform yielded sharp tunneling tips with 75 μm in baseline and 50 μm in depth. The sensors were assembled and fixed with measurement circuits, after their electrodes were patterned with modified photolithography and Co film was deposited with e-beam evaporation. A natural frequency response of 1.3 kHz was observed, and a tunneling barrier height of 0.713 eV was tested. Due to the quadratic relation between magnetic force and the field, the sensor field response (7.0×10^6 V/T^2) was also quadratic. The noise voltage at 1 kHz is 0.2 mV, corresponding to a magnet field of 0.46×10^{-6} T. The bandwidth of this senor is 18 kHz. This new type of sensor platform is promising for the next generation of microsensing applications.**

***Index Terms*—Hot embossing, magnetic field sensor, MEMS, PMMA, tunneling sensor.**

I. Introduction

SINCE the Nobel Prize was awarded to Binnig and Rohrer for the first scanning tunneling microscope (STM) in 1986 [1], the idea of a highly sensitive displacement transducer utilizing electron tunneling effect has been actively investigated by researchers. In electron tunneling transducers, 1% change in a tunneling current between electrodes corresponds to a displacement fluctuation of less than 0.03 Å. The changes in current magnitude are easily detected using an electronic feedback control circuit with a high input-impedance operation amplifier. Moreover, the high sensitivity in displacement is independent of the lateral size of the electrodes since the tunneling current occurs between two atoms located at opposite electrode surfaces [2], [3]. Due to their small size and high sensitivity, micromachined tunneling transducers make it possible to fabricate miniaturized and inexpensive tunneling sensors with high performance such as accelerometers [4]–[7], magnetometers [8]–[10], infrared radiation sensors [11]–[13], chemical sensors [14], [15], and pressure sensors [16].

The first tunneling transducer was reported by Niksch and Binning in 1987 [17]. Since then, sensors with displacement resolution approaching 10^{-4} Å$/\sqrt{\text{Hz}}$ have been fabricated by Waltman and Kaiser [18], where the displacement of a cantilever with a proof mass was measured through the tunneling current. The accelerometer had a bandwidth of 3 kHz and a resolution of about 1 μg$/\sqrt{\text{Hz}}$(1 g = 9.8 m/s^2). In 1994, Rockstad and his co-workers built a micromachined tunneling accelerometer for underwater acoustics applications with a resolution of 0.1 μg$/\sqrt{\text{Hz}}$ [19], and Yeh and Najafi developed a tunneling accelerometer with a low-voltage biased CMOS feedback circuit, demonstrating a resolution of 0.1–4 μg$/\sqrt{\text{Hz}}$ [20]. In 2001, Liu and his colleagues reported an accelerometer with the highest resolution so far, which is 0.02 μg$/\sqrt{\text{Hz}}$ with a bandwidth of 5 to 1.5 kHz [21]. Other types of micromachined physical sensors based on the tunneling effect have also been reported. Kenny and his co-workers reported a miniaturized infrared detector for thermal expansion of a trapped gas [22], [23]. MacDonald *et al.* [24]–[25] and Jiang *et al.* [26], [27] have demonstrated silicon tip arrays for various applications. The first tunneling magnetic field sensor was reported by Wandass and his fellow researchers [28]. They used a tunneling transducer to measure the elongation or contraction of a metallic glass ribbon in response to a changeable magnetic field, and reported a resolution of 2000 nT$/\sqrt{\text{Hz}}$ at 1 Hz. Brizzolara improved the sensor and had achieved a magnetic field resolution of 6 nT$/\sqrt{\text{Hz}}$ at 1 Hz [29]. The latter results [30], [31] showed that the magnetrostrictive strain could also be measured. Dilella [32] demonstrated a magnetometer with a resolution of 0.3 nT$/\sqrt{\text{Hz}}$ at 1 Hz using the torsion arm at an ambient temperature. However, the above tunneling transducers were based on silicon materials, and the micromachining process was time-consuming and the yield was low. New materials suitable for quick, easy micromachining, batch production, and low cost need to be investigated.

Manuscript received April 28, 2004; revised April 26, 2005. This work was supported in part by the National Science Foundation/LEQSF under Grant (2001-04)-RII-02, in part by DARPA under Grant DAAD19-02-1-0338, and in part by NASA under Grant (2002)-Stennis-22. The associate editor coordinating the review of this paper and approving it for publication was Dr. Andre Bossche.

J. Wang and W. Xue are with the Institute for Micromanufacturing, Louisiana Tech University, Ruston, LA 71272 USA (e-mail: wangjin2@seas.upenn.edu; xuewei@me.umn.edu).

N. V. Seetala is with the Department of Physics, Grambling State University, Grambling, LA 71245 USA (e-mail: naidusv@gram.edu.).

X. Nie is with the Department of Mechanical Engineering, Louisiana State University, Baton Rouge, LA 70803 USA, and also with the Department of Mechanical, Automotive, and Materials Engineering, University of Windsor, Windsor ON N9B 3P4 Canada (e-mail: xnie@uwindsor.ca).

E. I. Meletis is with the Department of Mechanical Engineering, Louisiana State University, Baton Rouge, LA 70803 USA, and also with the Department of Materials Science and Engineering, University of Texas at Arlington, Arlington, TX 79019 USA (e-mail: meletis@mae.uta.edu).

T. Cui was with the Institute for Micromanufacturing, Louisiana Tech University, Ruston, LA 71272 USA. He is now with the Department of Mechanical Engineering, University of Minnesota, Minneapolis, MN 55445 USA (e-mail: tcui@me.umn.edu).

Digital Object Identifier 10.1109/JSEN.2005.860366

In recent years, PMMA, a synthetic elastomer, has drawn much attention from many researchers. Its main advantages include low cost, low processing temperature, easy bond, and biocompatibility. These priorities make PMMA more preferable over silicon in the areas such as biological and medical applications.

In this paper, the polymer material (PMMA) is used to fabricate inexpensive, batch-fabricated, high-yield, and highly sensitive magnetic field sensors based on our previous tunneling sensor platform [33]. Hot embossing was employed as the micromachining technique due to its simplicity, fast fabrication speed, high yield, and high resolution. Taking advantage of the thermoplastic properties of PMMA, a micromachined, wide-bandwidth magnetic field sensor has been successfully constructed. The mechanical structure responses and the sensor performance are also reported and discussed thereafter.

II. Operation Methodology

The schematic cross section of the magnetic field sensor is shown in Fig. 1. The PMMA magnetic field sensor includes mechanical components and three electrodes. The mechanical components are composed of a membrane with a ferromagnetic film at the top surface and a tunneling tip opposite to the film at the bottom. The electrodes include a tip electrode, a counter electrode under ferromagnetic film, and a deflection electrode. The titanium/gold bi-layer is chosen as the electrode metal for its inert chemical characteristics as well as the relatively high work function of gold. When operating at the closed-loop mode, the sensor maintains a constant tip-to-membrane distance by applying an electrostatic feedback force on the deflection electrode.

The metallic tip electrode and the counter electrode form a tunneling junction. Usually, the voltage of the junction is biased at about 300 mV. At the constant distance mode, the gap between the tip and the counter electrode is about 10 Å, which is set by the DC voltage. The tunneling current I varies exponentially with the gap change z. The relationship between the tunneling current and the displacement change is

$$I = I_o \exp(-\alpha z \sqrt{\Phi}) \tag{1}$$

where Φ [eV] is the height of the tunneling barrier, I_o is the original tunneling current (about 1.5 nA), and α is a constant of 1.025. It can be derived and given by

$$\frac{d(\ln I)}{\mathrm{dz}} = \mathrm{const} \tag{2}$$

which means that the exponential relationship between the tunneling current and the separation gap can be achieved by measuring the slope of the semilog plot of the tunneling current versus the gap change. More detailed descriptions about the tunneling structures and the operation principles can be found in [7]–[33].

Based on the electron tunneling effect, we have built the all-PMMA-based tunneling sensor platform as displacement transducers [34]. The linear slope between the output voltage and the distance change between the tip and the counter electrode

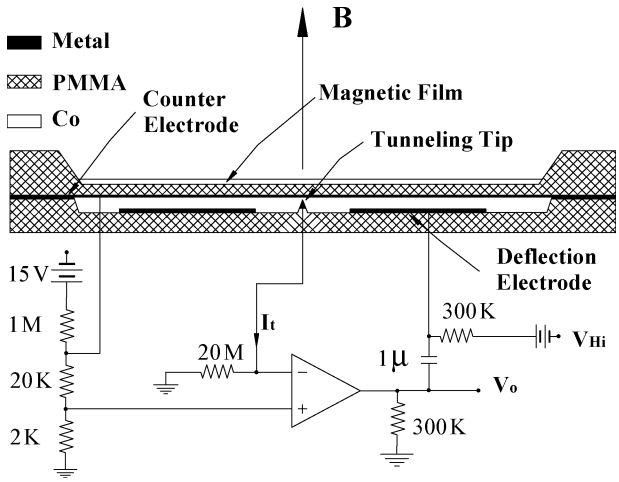

Fig. 1. Schematic diagram of the micromachined magnetic-field tunneling sensor. A feedback and control circuit is illustrated with the membrane structures. The synthesis of the circuit can be found in [33].

is about dV/dz$= 2 \times 10^7$ V/m. In the magnetic field sensor, the displacement changes are caused by the ferromagnetic force when alternating field is applied to the membrane. For a flat circular plate with a constant thickness, we defined D as the plate constant

$$D = \frac{Et^3}{12(1-v^2)} \tag{3}$$

where E is the Young's Modulus, t is the membrane thickness, and v is the Poisson's ratio. The displacement change at the circular center induced by a uniform pressure is

$$z = \frac{qr^4}{64D} \tag{4}$$

where z is the vertical deflection of plate at the center, r is the outer radius, and q is the load per unit area [35]. Actually, q can be rewritten as $q = F/\pi r^2$. The transfer function between the output voltage V and the ferromagnetic force F is derived as

$$\begin{aligned} \frac{\mathrm{dV}}{\mathrm{dF}} &= \frac{\mathrm{dV}}{\mathrm{dz}} \cdot \frac{\mathrm{dz}}{\mathrm{dF}} = 2 \times 10^7 \ \mathrm{V/m} \cdot \frac{r^2}{64\pi D} \\ &= 3 \times 10^7 \ \mathrm{V/m} \cdot \frac{(1-v^2)}{8\pi E} \cdot \frac{r^2}{t^3}. \end{aligned} \tag{5}$$

From the above analysis, the output voltage of the sensor is proportional to the magnetic force applied to the magnetic film. The magnitude of the transfer function is determined by the radius and the thickness of the membrane. On the other hand, because the Young's Modulus of PMMA is about 3.9 GPa, which is about 1/45 of silicon's value of 179 GPa [36], the transfer function of a PMMA sensor is rather large compared with a silicon sensor if the structures remain the same. This is the main reason why polymer is selected as the alternative material instead of silicon.

III. Fabrication Process

The structures of the all-PMMA-based tunneling magnetic sensors were built with the hot embossing replication followed by RIE to reduce the membrane thickness. Due to the repeated

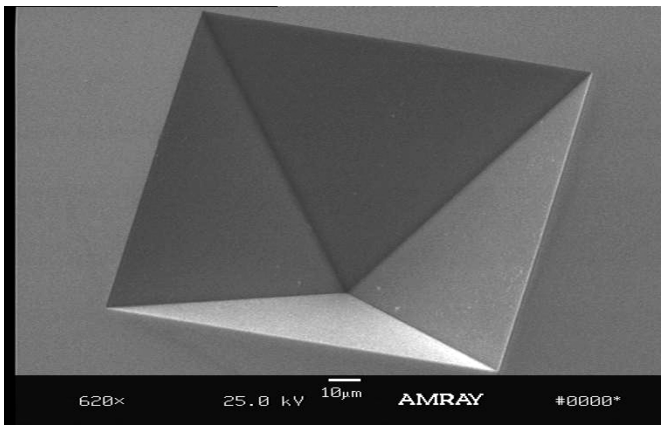

Fig. 2. SEM micrograph of pyramid tunneling tip pit on silicon template. The edges are sharp and the surface is smooth, which is suitable for hot embossing demolding. The tip pit is 75 μm at edge and 50 μm in depth.

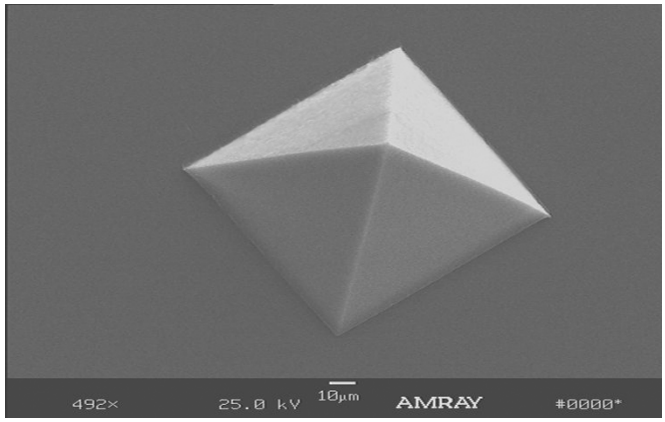

Fig. 3. SEM micrograph of PMMA tunneling tip replicated by hot embossing. The tip has smooth surface and sharp edges with base line of 75 μm and height of 50 μm.

usage of templates in the hot embossing, the cost of mold fabrication can be inexpensive in the whole process. The mass replication of structures from a template to PMMA substrates makes PMMA an excellent choice for industrial mass production. In addition, the whole turn-around for such a replication is less than 20 min, considerably faster compared with the silicon processing. Moreover, there is almost no lateral feature size limitation to the hot embossing. The line width limitation comes from the availability of the mold itself [37]. In addition, the hot embossing is a single-step process, and it consumes fewer chemicals and needs fewer instruments. With a well-developed, sharp angle, smooth surface, and high-aspect-ratio silicon mold, the sensors features were easily replicated within 20 min. For the hot embossing technique, the key factor of structure construction is the silicon mold because there is almost no feature size loss if the fabrication conditions are under strict control.

A. Silicon Molds Fabrication

Two silicon templates are needed, one for the top part and the other for the bottom part of the sensor. The preparation of silicon templates for the hot embossing starts with KOH wet etching with silicon dioxide (SiO_2) as the etching mask. After the anisotropic etching, the SiO_2 layer was removed before the silicon template was thoroughly cleaned, which was followed by an anodic bonding to a Pyrex glass. A SEM micrograph of a silicon pit on a mold is shown in Fig. 2, in which the sidewall of the pyramid is smooth and the four edges are sharp. The detailed description can be found in [38].

B. Structure Replication by Hot Embossing

A hot embossing machine (HEX 01/LT from Jenoptik Microtechnik GmbH, Inc.) was used for a fast, simple, and mass replication process. When using the hot embossing for structure replication, a polymer substrate was laid onto the bottom heating plate of the embossing machine, and the surrounding vacuum chamber was closed. Next, the heated mold insert was pressed into the softened polymer under vacuum. After a subsequent cooling, demolding took place by removing the plastic part from the mold. The demolding process is more important because sometimes the microstructures were destroyed by either cracking the mold or the friction of the sidewall. According to the data in [39], the glass temperature of PMMA is about 100 °C to 105 °C and the melting temperature is about 112 °C to 130 °C. Therefore, the molding temperature was adjusted to 165 °C, higher than the melting temperature. When the molding was in progress, the chamber was compressed down, with a maximum contact force of 20 kN. The background pressure was about 1.5 mbar. The template was held on the PMMA substrate for about 60 s, and then the temperature was cooled down. The demolding system was designed to overcome the holding forces between the mold and the PMMA substrate with the aid of pressurized air, which was applied from the top of a mold holder. In our case, the demolding temperature was set at 80 °C. The speed of the moving mold is 1 mm/min. The templates, with 40 cell units, can be used for 20 to 25 times before the quality of the product deteriorates.

The fabricated PMMA pyramid tip is shown in Fig. 3. The tip consists of four smooth surfaces, a sharp tip point, and four steep edges, which can compete with tunneling tips acquired by micromachining on silicon, even though very sharp tips are not required for tunneling sensors [40].

The fabrication of top part of the sensor is also important. As analyzed earlier in (5), the magnitude of the sensor transfer function is proportional to the outside radius of the sensor, and is reversely proportional to the membrane thickness of the sensor. In addition, the natural frequency response of the circular flat membrane relates with the thickness and outer radius [41], and given by

$$f = \frac{k_1}{2\pi}\sqrt{\frac{Dg}{qr^4}} = \frac{K_1}{2\pi}\sqrt{\frac{E}{12(1-v^2)}}\frac{t}{r^2} \tag{6}$$

where k_1 is 10.2, a constant for fundamental natural frequency. A relative high natural frequency is preferable because it determines the bandwidth of the sensor. The relationship among transfer function magnitude $|dV/dF|$, sensor radius r, and membrane thickness t were simulated by ANSYS [42], and the t and r values were synthesized as 20 μm and 4 mm, respectively. After structure replication of the top part of the sensor by hot embossing, the thickness of the sensor membrane was

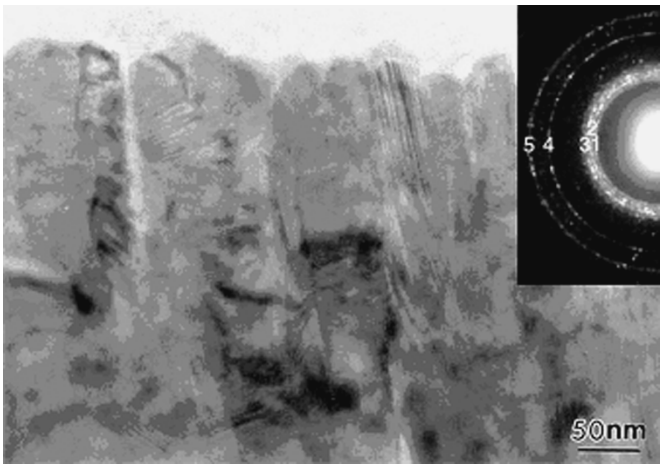

Fig. 4. Cross-sectional TEM image of the Co thin film deposited on the PMMA substrate.

tested. When using a PMMA sheet with original thickness of 500 μm, the embossed membrane was about 200 μm thick. Reactive ion etching was used to reduce the membrane thickness into targeted thickness. The flowrates of reactive gases of O_2 and SF_6 were 12 and 2.5 sccm, respectively, with a pressure of 280 mTorr. The etching process was performed intermittently to ensure that the PMMA sheet was fully cooled down. The etching power was 200 W, which produced an etching rate of about 1 μm per minute. The total etching time was 180 min, resulting in a membrane thickness of 20 μm. Finally, the Ti/Au bi-layer was sputtered on the back surface and a layer of pure Co thin film was deposited by e-beam evaporation. During the deposition, the "bank area" (thick part of the unit) was covered by a metal mask, which also facilitated the heat transferring. The detailed description of structure design, simulation and characteristic of the PMMA tunneling sensor can be found in [43].

C. Deposition of Ferromagnetic Co Film

An electron beam vapor deposition system (Edwards Auto 306) was used to synthesize a crystalline Co thin film [44]. A 200-nm-thick Co thin film was obtained after 160 min deposition. Transmission electron microscopy (JEOL 2010) was used for microstructural characterization. The crystallographic structure of the Co was determined by electron diffraction analysis. Fig. 4 shows a cross-sectional TEM image of the pure Co film. A columnar structure with a column width of 20–30 nm and a length equal to the entire film thickness was observed in the Co film. The crystal structure of the film can be identified as hexagonal α-Co with lattice parameters $\boldsymbol{a} = 2.501$ Å and $\boldsymbol{c} = 4.066$ Å, as shown in the selected-area electron diffraction (SAED) pattern in the inset. The five diffraction rings in the inset (Fig. 4) correspond to a lattice spacing of 2.17 Å, 2.07 Å, 1.92 Å, 1.25 Å, and 1.07 Å that can be indexed as the (100), (002), (101), (110), and (112) reflection, respectively.

D. Assembly and Measurement

The replicated upper and lower sheets of all-PMMA tunneling sensor are shown in Fig. 5(a) and (b). The two sheets were bonded together central symmetrically using stereo microscope (Olympus SZ40). The wire-electrode bonding was implemented by electrical conductive adhesive (silver epoxy kit). The two-part silver epoxy was an electrically conductive silver filled epoxy adhesive, which was recommended for a wide range of electronic bonding and sealing applications. The bonding shows a combination of good mechanical and electrical properties. The two-part smooth paste formulation of refined pure silver and epoxy was free of solvents and copper or carbon additives. The assembled sensor was then fixed onto an 18-pin socket, as shown in Fig. 5(c). The dimension of the sensor is $8 \times 8 \times 2$ mm, excluding the socket. An AC field was inspirited by a solenoid coil with AC current. The parameters of the solenoid coil and the magnetic fields produced by it were listed in Table I. A Gaussian meter (model 100) was used for field calibration.

The measurement circuit was built with a simple, yet effective, modeling method with a system linearization at small signal input approximation. The purpose of the control and feedback circuits is to broaden the bandwidth, enhance the system stability, and optimize the mechanical damping. The details on how to analyze the function model, linearize the tunneling effect, and build the circuit were given in [33] and [34].

IV. Results and Discussions

A. Mechanical Structure Properties

The vibration responses of frequencies were examined at AC field application. The Polytec Laser Vibrometer VDD 650 system was used to measure nano-scale displacement changes. The magnetic field magnitude was kept constant by monitoring the excitation coil current. The vibration amplitude versus excitation frequency was plotted in Fig. 6. The sharp peak corresponds to the natural frequency of $f_o = 1.3$ kHz. According to (6), the thickness of membrane was derived as 23.3 μm ($E = 3.9$ GPa, $v = 0.3$), which is consistent with the expected value of 20 μm.

B. Tunneling Effect Measurement

The tunneling current was measured with the aid of the Laser Vibrometer. At open loop status, a high DC voltage was applied on the deflection electrode, which set the gap between the tunneling tip and the counter electrode to about 1 nm. An ac field with a frequency lower than the natural frequency f_o was applied on the sensor. The excited force produced a small vibration. The value of tunneling current was obtained through a high impedance amplifier. The relationship between the displacement changes and the induced current is plotted in Fig. 7. The fitted line in the semilog plot exhibits the effective barrier height of $\Phi = 0.173$ eV, which is rather similar to the values in other groups [45].

C. Characteristics of the Sensor

The relationship between the sensor output voltages and the applied fields is shown in Fig. 8. The curves were fitted into polynomial expressions

$$V = aB^2 + bB + c \tag{7}$$

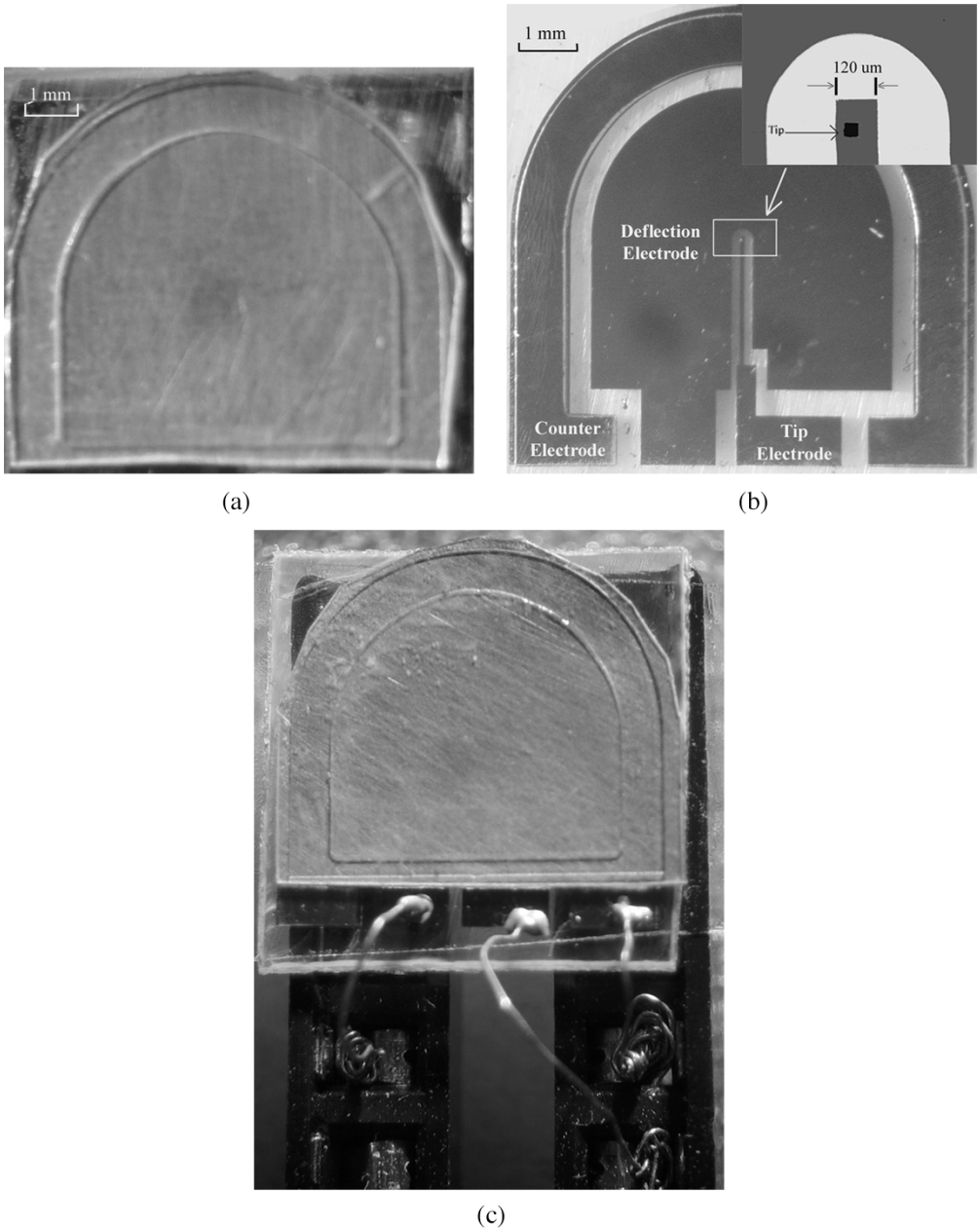

Fig. 5. Photographs of the top view of all-PMMA magnetic tunneling sensor. (a) The top sheet was produced by hot embossing. The thickness of the Co thin film at the top surface is 200 nm and the thickness of the metallic bi-layer of Pt/Au was 30 and 70 nm, respectively. In (b) is the patterned lower sheet of sensor. The three electrodes are comprised of Pt/Au films. The inset picture is a close look of the tunneling tip. After the top and lower sheets were bonded together, the three electrodes were connected with measuring wires by Epoxy adhesive and the sensor was set onto IC socket in (c).

where a, b, and c are fitted constant, but change as functions of field frequency. The nonlinear plot comes from the nonlinear force-field relation. Based on the magnetic energy gradient change, the relationship between the magnetic field and the magnetomotive force is derived as [46]

$$F = \frac{B^2 A}{2\mu_0} \tag{8}$$

where A is the overlap area in field, and μ_0 is the permeability in the air. Considering (5), (8), and $\mathrm{dV/dB} = (\mathrm{dV/dF}) \cdot (\mathrm{dF/dB})$, the transfer function of the sensor is

$$V = 2 \times 10^7 \ \mathrm{V/m} \cdot \frac{r^2}{64\pi D} \cdot \frac{A}{2\mu_0} \cdot B^2 + c. \tag{9}$$

Compared with (7), the theoretical value of a is $6.9 \times 10^6 \ \mathrm{V/T^2}$.

A $V - B$ plot at different frequencies was examined, and a and b values are given as line (a) and (b) in Fig. 9, respectively. For line (a), the factor a keeps a consistent value when the frequency is lower than 18 kHz. At higher frequencies, the a values decrease quickly, which produces a cut-off frequency of 18 kHz. As analyzed by the theory above, the measurement value of $7.0 \times 10^6 \ \mathrm{V/T^2}$ is almost the same as the prediction. However, factor b as the frequency responses can not be explained by the simple theoretical analysis directly.

Reconsidering (7) gives

$$V = a\left(B + \frac{b}{2a}\right)^2 + c' \tag{10}$$

TABLE I
SOLENOID COIL SPECIFICATIONS

Parameters	Observed
Dimension	30 mm × 30 mm × 48 mm
Turns	300
Resistor (Ω)	0.8
Max. Current (A)	0.4
Field Calculated	7.85×10^{-3} T/A
Field Measured [a]	9.50×10^{-3} T/A

[a] A ferromagnetic metal core is inserted

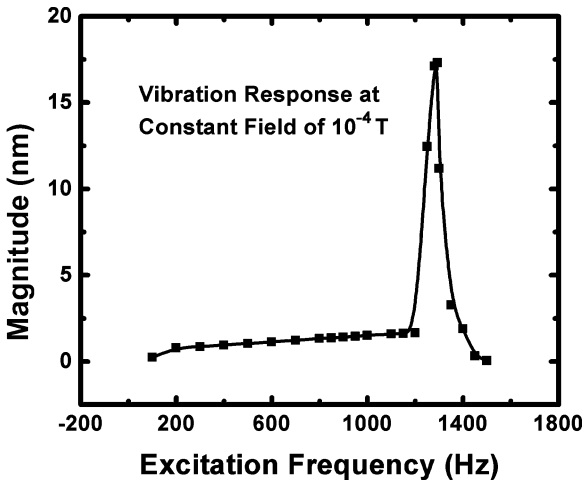

Fig. 6. Vibration response as a function of frequency changes. The magnetic field was kept at constant of 10^{-4} T.

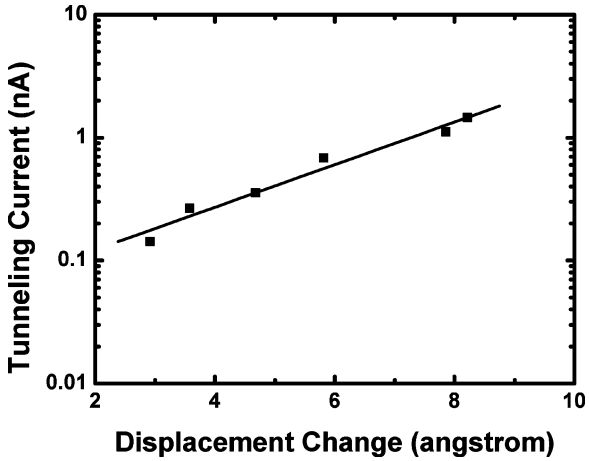

Fig. 7. Tunneling current plot for all-PMMA magnetic sensor. The slope of fitted line between log current and displacement change is 0.173 eV.

where c' is another constant. The ratio $b/2a$, plotted in Fig. 10, describes the field shifting at different frequencies. From the distribution in Fig. 10, the changes of $b/2a$ values are divided

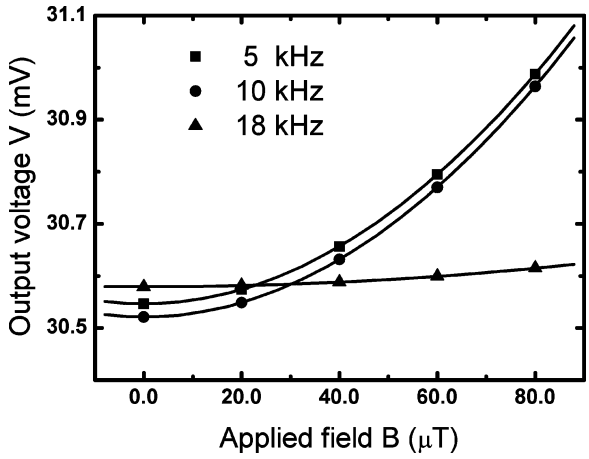

Fig. 8. Output of magnetic sensor dependence on applied field. Three plots correspond to 5-, 10-, and 18-kHz AC field. The curves can be expressed as $V = aB^2 + bB + c$, where a, a, and c vary depending on frequency.

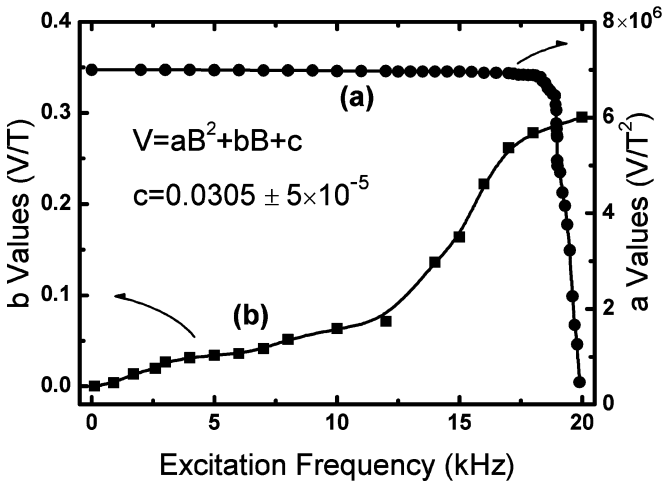

Fig. 9. Measurement of a and b values as a function of frequency. The factor a keeps almost constant when frequency is lower than 18 kHz and it drops quickly after this cut off frequency. The factor b increases slowly with the frequency rise.

into three areas. When the frequency is lower than 2 kHz, the ratio increases quickly to a level of about 1×10^{-9} T, which is about 0.01 mG. This small value can be regarded as environment field shift because it is about 2% of the earth's field level (about 0.5 mG). When frequency increases from 2 to 18 kHz, the $b/2a$ ratio increases slowly from 0.01 to 0.2 mG, almost half of the earth's field. The field shift results from the interaction among the feedback electrostatic force, the field fluctuation, and the Co thin film because at a frequency larger than natural response ($f_o = 1.3$ kHz), the counter balance force between the electrodes will produce some flux traps in the Co film, which cause the field shift. At a frequency larger than 18 kHz, the field shift increases quickly, and turns into a level of several mG. The frequency, where field shift grows quickly, is called "corner frequency." The sensor cannot function well beyond the corner frequency.

The constant value c, $0.0305\pm5\times10^{-5}$ V, is the sensor zero. It cannot be completely ignored due to the fact that nonfield-shield environment can lead to some trapped flux movement.

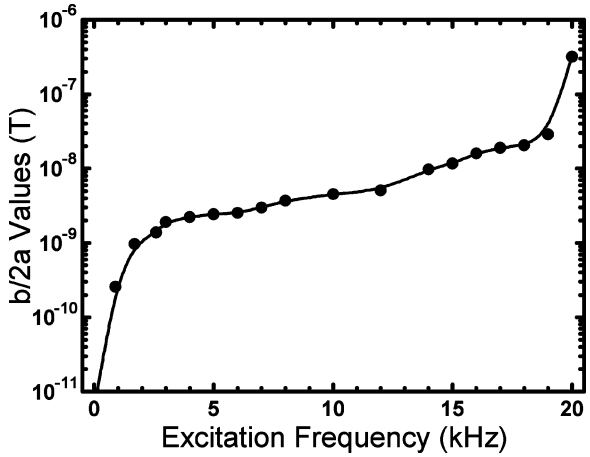

Fig. 10. Plot of $b/2a$ ratio dependent on frequency change. The circles are measured values and the line is fitted curve. The ratio changes can be divided into three parts: from DC to 2 kHz, from 2 kHz to 18 kHz, and larger than 18 kHz.

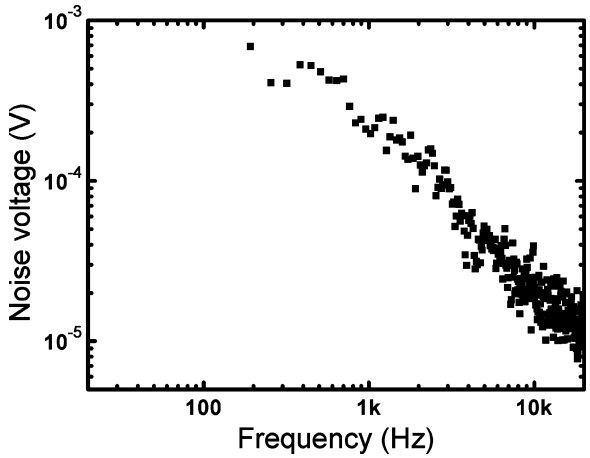

Fig. 11. Noise voltage spectrum plot. The voltage at 1 kHz is about 0.2 mV, which produces a resolution of 2.13×10^{-13} T$^2/\sqrt{\text{Hz}}$ when considering the bandwidth of 18 kHz and transfer function factor of 7.0×10^6 V/T^2.

D. Noise Measurement

The measurement of noise voltage is performed by PULSE Multi-analyzer System Type 3560. When applied magnetic field was tuned to zero, output voltage noise spectrum was observed. Fig. 11 illustrates the noise voltage spectrum of our fabricated magnetic sensor. The measured noise level at 1 kHz is about 0.2 mV, which corresponds to the sensor noise level of 2.13×10^{-13} T$^2/\sqrt{\text{Hz}}$. This value is not a real "field resolution" because it only describes a "field square resolution." It is hard to compare this value with other types of silicon-based magnetic sensors. However, the all-PMMA-based tunneling magnetic sensors have proved a potential to demonstrate a resolution better than the order of μT. Either by structure modification or measurement circuit enhancement, the linear relationship between the output voltage and the applied field will be obtained. A summary of sensor performance is listed in Table II.

TABLE II
DEVICE PARAMETERS

Parameter	Specifications
Dimension	8 mm × 8 mm × 2 mm
Magnetic thin film	Co (98%), 200 nm
Membrane area	50.24 mm^2
Membrane thickness	20 μm
Bias voltage, V_{bias}	300 mV
Transfer factor, a	$7.0\times10^6\, V/T^2$
Resonant frequency, f_o	1.3 *kHz*
Barrier height, Φ	0.173 eV
Bandwidth, B	18 *kHz*
Noise level	$2.13\times10^{-13}\, T^2/\sqrt{Hz}$

V. CONCLUSION

All polymer tunneling magnetic sensors with a broad bandwidth were successfully fabricated based on the PMMA tunneling sensor platform. The hot embossing technique, one of the most important micromachining approaches in "soft-lithography," showed its advantages of fast turn-around, less processing parameters, and simplicity. Compared with traditional silicon-based tunneling sensors, the PMMA-based structures have advantages such as less stiffness, lower cost, and easier fabrication. Because the mold can be used repeatedly, the potential of mass-production is possible. The characterization of the polymeric microsensors indicates that the PMMA-based tunneling magnetic sensor represents a promising micro device so that it could be further developed as the next generation of highly sensitive microsensors.

ACKNOWLEDGMENT

The authors would like to thank J. Fang for the ICP processing.

REFERENCES

[1] G. Binning and H. Rohrer, "Scanning tunneling microscopy," *IBM J. Res. Develop.*, vol. 30, pp. 355–369, 1986.
[2] M. F. Bocko, K. A. Stephenson, and R. H. Koch, "Vacuum tunneling probe: a nonreciprocal, reduced-back-action transducer," *Phys. Rev. Lett.*, vol. 61, pp. 726–729, 1988.
[3] M. F. Bocko and K. A. Stephenson, "Tunneling transducers: quantum limited displacement monitors at the nanometer scale," *J. Vac. Sci. Technol. B*, vol. 9, pp. 1363–1366, 1991.
[4] T. W. Kenny, J. K. Reynolds, W. J. Kaiser, T. R. VanZandt, and T. B. Gabrielson, "Miniature high-resolution accelerometer utilizing electron tunneling," in *Proc. American Society of Mechanical Engineers, Dynamic Systems and Control Division*, vol. 40, 1992, pp. 41–52.
[5] H. K. Rockstad, T. W. Kenny, J. K. Reynolds, W. J. Kaiser, and T. B. Gabrielson, "A miniature high-sensitivity broad-band accelerometer based on electron tunneling transducers," *Sens. Actuators A*, vol. 43, pp. 107–114, 1994.
[6] P. M. Zavracky, B. McClelland, J. Wang, and F. T. Hartley, "Tunneling tip protection for a bulk micromachined accelerometer," *Proc. SPIE*, vol. 2639, pp. 31–37, 1995.
[7] P. R. Scheeper, J. K. Reynolds, and T. W. Kenny, "Development of a modal analysis accelerometer based on a tunneling displacement transducer," in *Proc. Int. Conf. Solid-State Sensors and Actuators*, vol. 2, 1997, pp. 867–870.

[8] L. M. Muller, J. A. Podosek, E. Kruglick, T. W. Kenny, J. A. Kovacich, and W. J. Kaiser, "μ-magnetometer based on electron tunneling," in *Proc. IEEE Micro Electro Mechanical Systems*, 1996, pp. 467–472.
[9] J. Zhu, Z. Zhou, H. Ding, and X. Ye, "Fabrication of micro tunneling magnetometer and on-wafer test," in *Proc. Int. Symp. Test and Measurement*, vol. 1, 2001, pp. 11–13.
[10] M. Tondra, A. Jander, and C. Nordman, "Low-power 3-axis magnetometers using spin dependent tunneling for UGS and security applications," *Proc. SPIE*, vol. 4743, pp. 188–196, 2002.
[11] T. W. Kenny, W. J. Kaiser, J. A. Podosek, H. K. Rockstad, and J. K. Reynolds, "Micromachined electron tunneling infrared sensors," in *Proc. IEEE Tech. Dig. Solid-State Sensor and Actuator Workshop*, 1992, pp. 174–177.
[12] T. W. Kenny, "Tunneling infrared sensors," *Semicond. Semimetals*, vol. 47, pp. 227–266, 1997.
[13] J. Grade, A. Barzilai, J. K. Reynolds, C. H. Liu, A. Partridge, H. Jerman, and T. W. Kenny, "Wafer-scale processing, assembly, and testing of tunneling infrared detectors," in *Proc. Int. Conf. Solid-State Sensors and Actuators*, vol. 2, 1997, pp. 1241–1244.
[14] I. Read, A. M. Napper, N. J. Head, A. M. Oliver, M. J. Shephard, M. N. PaddonRow, and D. H. Waldeck, "Use of U-shaped donor-bridge-acceptor molecules to study electron tunneling through nonbonded contacts," *J. Amer. Chem. Soc.*, vol. 124, no. 34, pp. 10 171–10 181, Aug. 28, 2002.
[15] K. S. Nakayama, E. Graugnard, and J. H. Weaver, "Tunneling electron induced bromine hopping on $\mathrm{Si}(100)-(2\times 1)$," *Phys. Rev. Lett.*, vol. 89, no. 26, pp. 266 106/1–266 106/4, Dec. 2002.
[16] R. C. White, T. Long, and T. W. Schneider, "Development of miniature electro-mechanical pressure sensor arrays (MEMPSA) for high resolution thermospheric and mesospheric neutral wind measurement," *Proc. SPIE*, vol. 4205, pp. 248–259, 2001.
[17] M. Niksch and G. Binnig, "Proposal for a novel gravitational-wave sensor," *J. Vac. Sci. Technol. A*, vol. 6, pp. 470–471, 1988.
[18] S. B. Waltman and W. J. Kaiser, "An electron tunneling sensor," *Sens. Actuators*, vol. 19, pp. 201–210, 1989.
[19] H. K. Rockstad, T. K. Tang, J. K. Reynolds, T. W. Kenny, W. J. Kaiser, and T. B. Gabrielson, "A miniature, high-sensitivity, electron tunneling accelerometer," *Sens. Actuators A*, vol. 53, pp. 227–231, 1996.
[20] C. Yeh and K. Najafi, "A low-voltage bulk-silicon tunneling -based micro accelerometer," in *Proc. Int. Electron Device Meeting Dig.*, 1995, pp. 23.1.1–23.1.4.
[21] C. H. Liu and T. W. Kenny, "A high-precision, wide-bandwidth micromachined tunneling accelerometer," *J. Microelectromech. Syst.*, vol. 10, no. 3, pp. 425–433, Sep. 2001.
[22] T. W. Kenny, W. J. Kaiser, S. B. Waltman, and J. K. Reynolds, "Novel infrared detector based on a tunneling displacement transducer," *Appl. Phys. Lett.*, vol. 59, pp. 1820–1822, 1991.
[23] T. W. Kenny, J. K. Reynolds, J. A. Podosek, E. C. Vote, L. M. Miller, H. K. Rockstad, and W. J. Kaiser, "Micromachined infrared sensors using tunneling displacement transducers," *Rev. Sci. Instrum.*, vol. 67, pp. 112–128, 1996.
[24] J. J. Yao, S. C. Arney, and N. C. MacDonald, "Fabrication of high frequency two-dimensional nanoactuators for scanned probe devices," *J. Microelectromech. Syst.*, vol. 1, no. 1, pp. 14–22, Mar. 1992.
[25] N. C. MacDonald, "Single crystal silicon nanomechanisms for scanned-probe device arrays," in *Proc. IEEE Solid-State Sensor and Actuator Workshop Tech. Dig.*, 1992, pp. 1–5.
[26] J. C. Jiang, R. C. White, and P. K. Allen, "Microcavity vacuum tube pressure sensor for robot tactile sensing," in *Proc. Transducers*, 1991, pp. 238–240.
[27] J. C. Jiang, V. Faynberg, R. C. White, and P. K. Allen, "Fabrication of micromachined silicon tip transducer for tactile sensing," *J. Vac. Sci. Technol., B*, vol. 11, pp. 1962–1967, 1993.
[28] J. H. Wandass, J. S. Murday, and R. J. Colton, "Magnetic field sensing with magnetostrictive materials using a tunneling tip detector," *Sens. Actuators*, vol. 19, pp. 211–225, 1989.
[29] A. Robert, R. J. Colton, M. Wun-Fogle, and H. T. Savage, "Tunneling-tip magnetometer Brizzolara," *Sens. Actuators*, vol. 20, no. 3, pp. 199–205, Dec. 1, 1989.
[30] R. A. Brizzolara and R. J. Colton, "Magnetostriction measurements using a tunneling-tip strain detector," *J. Magn. Magn. Mater.*, vol. 88, no. 3, pp. 343–350, Aug. 1990.
[31] R. A. Brizzolara and R. J. Colton, "The magnetostriction of CoFeNiMo metallic glasses measured with a tunneling transducer," *J. Magn. Magn. Mater.*, vol. 103, pp. 111–116, 1992.
[32] D. DiLella, L. J. Whitman, R. J. Colton, T. W. Kenny, W. J. Kaiser, E. C. Vote, J. A. Podosek, and L. M. Miller, "Micromachined magnetic-field sensor based on an electron tunneling displacement transducer," *Sens. Actuators A*, vol. 86, no. 1–2, pp. 8–20, Oct. 2000.
[33] J. Wang, "Vertical Polymer Tunneling Sensor Platform by Hot Embossing Technique," Ph.D. dissertation, Inst. Micromanufact., Louisiana Tech Univ., Ruston, 2003.
[34] J. Wang, Y. Zhao, T. Cui, and K. Varahramyan, "Synthesis of the modeling and control systems of a tunneling accelerometer using the MatLab simulation," *J. Micromech. Microeng.*, vol. 12, no. 6, pp. 730–735, Nov. 2002.
[35] W. C. Young, *Roark's Formulas for Stress and Strain, Formula 10.b, Table 24*, 6th ed. New York: McGraw-Hill, 1989.
[36] B. Bhushan and X. Li, "Micromechanical and tribological characterization of doped single-crystal silicon and polysilicon films for microelectromechanical systems devices," *J. Mater. Res.*, vol. 12, no. 1, pp. 54–63, 1997.
[37] S. R. Quake and A. Scherer, "From micro- to nanofabrication with soft materials," *Science*, vol. 290, pp. 1536–1540, 2000.
[38] J. Wang, W. Xue, and T. Cui, "A combination technique to fabricate hot embossing master for PMMA tunneling transducers," *Microsyst. Technol.: Sens., Actuators, Systems. Integr.*, vol. 10, pp. 329–333, 2004.
[39] M. A. Karabeyoglu and D. Altman, "Dynamic modeling of hybrid rocket combustion," *J. Propuls. Power*, vol. 15, no. 4, pp. 562–571, 1999.
[40] T. W. Kenny, W. J. Kaiser, H. K. Rockstad, J. K. Reynolds, J. A. Podosek, and E. C. Vote, "Wide-bandwidth electromechanical actuators for tunneling displacement transducers," *J. Microelectromech. Syst.*, vol. 3, no. 3, pp. 97–104, Sep. 1994.
[41] W. C. Young, *Roark's Formulas for Stress and Strain, Formula 10.a, Table 36*, 6th ed. New York: McGraw-Hill, 1989.
[42] W. Xue, J. Wang, and T. Cui, "Modeling and design of polymer-based tunneling accelerometers by ANSYS/MATLAB," *IEEE Trans. Mechatron.*, vol. 10, no. 4, pp. 468–472, Apr. 2005.
[43] J. Wang and T. Cui, "Design, simulation, fabrication, and characterization of a PMMA tunneling sensor based on hot embossing technique," *Microsyst. Technol.*, vol. 11, pp. 452–455, 2005.
[44] X. Nie, J. C. Jiang, L. D. Tung, L. Spinu, and E. I. Meletis, "Multifunctional Co-C nanocomposite thin films, thin solid films," *Thin Solid Films*, vol. 415, no. 1–2, pp. 211–218, Aug. 2002.
[45] C. H. Liu, A. M. Barzilai, J. K. Reynolds, A. Partridge, T. W. Kenny, J. D. Garde, and H. K. Rockstad, "Characterization of a high-sensitivity micromachined tunneling accelerometer with micro-g resolution," *J. Microelectromech. Syst.*, vol. 7, no. 2, pp. 235–244, Jun. 1998.
[46] R. L. Comstock, *Introduction to Magnetism and Magnetic Recording*. New York: Wiley, 1999.

Jing Wang received the B.S. and M.S. degrees in electrical engineering from the Department of Electrical Engineering, Nankai University, Tianjin, China, in 1993 and 1996, respectively, and the Ph.D. degree in electrical engineering from the Institute for Micromanufacturing, Louisiana Tech University, Ruston, in 2003.

Currently, he is a Postdoctoral Fellow at the Department of Mechanical Engineering and Applied Mechanics (MEAM), University of Pennsylvania, Philadelphia. From 1996 to 1999, he was a Research Engineer with the Institute of Physics, Chinese Academy of Sciences (CAS), Beijing. His research interests include microfabrication technologies, solid-state sensors and actuators, polymer microelectronics, μTAS, and bio-MEMS.

Wei Xue received the B.S. and M.E. degrees in electrical engineering from Shandong University, Jinan, Shandong, China, in 1997 and 2000, respectively. He is currently pursuing the Ph.D. degree in the Department of Mechanical Engineering, University of Minnesota, Minneapolis.

His main research interests include microfabrication techniques, nanotechnology, polymer MEMS, chemical and biological sensors, modeling, and system control.

Naidu V. Seetala received the Ph.D. degree from the Saha Institute of Nuclear Physics, India.

He is a Professor of physics at Grambling State University (GSU), Grambling, LA. He joined GSU as faculty in 1988. He served as visiting faculty at Argonne National Laboratory and the MINT Center, the University of Alabama, Tuscaloosa, and was a Research Associate/Lecturer at the University of Texas, Arlington, in 1986. His research interests include nanoparticles for magnetic storage media; magnetochemical studies of nanocatalysts for syngas conversion: sol-gel synthesis and micro-channel reactor studies; thermal spray coatings—interfaces and adhesion studies; magnetic thin films and multilayers; and radiation effects. He has directed several research grants supported by DOE, the National Science Foundation, AFOSR, and the Office of Naval Research. He has authored over 50 scientific research journal publications.

Xueyuan Nie received the Ph.D. degree from the University of Hull, Hull, U.K., in 2000.

He is an Assistant Professor at University of Windsor, Windsor, ON, Canada. His research deals with multifunctional nanomaterials, thin films and coatings, micro/nano-mechanics, and tribology. He was a Postdoctoral Fellow and Research Assistant Professor at Louisiana State University, Baton Rouge, from 2000 to 2003.

Efstathios I. Meletis received the undergraduate degree in chemical engineering from the National Technical University of Athens, Athens, Greece, and the M.Sc. and Ph.D. degrees in materials science and engineering from the Georgia Institute of Technology (GIT), Atlanta.

He held appointments at GIT, IIT Research Institute, University of California, Davis, and Louisiana State University, Baton Rouge, where he was an Endowed Professor of materials science and engineering. He is currently Professor and Director of materials science and engineering at The University of Texas, Arlington. His major research areas are in surface engineering, multifunctional thin films, small-scale materials, and material-environment interactions. His recent work focuses on multifunctional nanocomposite thin films, scale effects on material properties, self-assembling in inorganic materials, and nanofabrication. His research program has been funded by the National Science Foundation, NASA, ARO, DARPA, Lockheed Martin, and other federal and industrial sources.

Dr. Meletis has been a recipient of the William Fulbright Scholar Research Award.

Tianhong Cui received the B.S. degree from the Nanjing University of Aeronautics and Astronautics, Nanjing, China, in 1991, and the Ph.D. degree from the Chinese Academy of Sciences, China, in 1995.

He is currently a Nelson Associate Professor of mechanical engineering at the University of Minnesota, Minneapolis. From 1999 to 2003, he was an Assistant Professor of Electrical Engineering at Louisiana Tech University, Ruston. Prior to that, he was an STA Fellow at the National Laboratory of Metrology, and served as a Postdoctoral Research Associate at the University of Minnesota and Tsinghua University, China. His current research interests include MEMS/NEMS, nanotechnology, and polymer electronics.